Asymmetric transmitter binding sites of fetal muscle acetylcholine receptors shape their synaptic response

Tapan K. Nayak and Anthony Auerbach[1]

Department of Physiology and Biophysics, State University of New York, Buffalo, NY 14214

Edited by Jean-Pierre Changeux, Institut Pasteur, Paris, France, and approved July 3, 2013 (received for review May 1, 2013)

Neuromuscular acetylcholine receptors (AChRs) have two transmitter binding sites: at α–δ and either α–γ (fetal) or α–ε (adult) subunit interfaces. The γ-subunit of fetal AChRs is indispensable for the proper development of neuromuscular synapses. We estimated parameters for acetylcholine (ACh) binding and gating from single channel currents of fetal mouse AChRs expressed in tissue-cultured cells. The unliganded gating equilibrium constant is smaller and less voltage-dependent than in adult AChRs. However, the α–γ binding site has a higher affinity for ACh and provides more binding energy for gating compared with α–ε; therefore, the diliganded gating equilibrium constant at −100 mV is comparable for both receptor subtypes. The −2.2 kcal/mol extra binding energy from α–γ compared with α–δ and α–ε is accompanied by a higher resting affinity for ACh, mainly because of slower transmitter dissociation. End plate current simulations suggest that the higher affinity and increased energy from α–γ are essential for generating synaptic responses at low pulse [ACh].

allostery | cholinergic | nicotinic | kinetics

Vertebrate neuromuscular acetylcholine receptors (AChRs) are ligand-gated ion channels comprised of five subunits: two α(1) and one each of β, δ, and either γ or ε. In most species, the γ-subunit is replaced by ε during postnatal development. Electrical activity in muscle cells induced by the neurotransmitter acetylcholine (ACh) is important for the molecular maturation of γ- to ε-AChRs (1, 2).

Without γ-subunit, neuromuscular synapses do not develop properly (3) and are abnormal in innervation patterns (4) and muscle fiber-type composition (5). In mice, the γ-subunit KO is lethal (6), and in humans, mutations in the *cholinergic receptor*, *nicotinic*, *gamma* (*CHRNG*) gene that encodes for γ-subunit are associated with lethal forms of multiple pterygium and Escobar syndromes (7–9).

AChRs have two transmitter binding sites located in the extracellular domain at α–δ and α–γ/ε-subunit interfaces. In adult AChRs, the α–δ and α–ε sites are equal and independent insofar as each has the same affinity for ACh and supplies the same amount of binding energy for gating (10). In fetal AChRs, the two binding sites are asymmetric with regard to agonist affinity, with estimates for the ratio of resting equilibrium dissociation constants for ACh ranging from ∼5- (11, 12) to >100-fold (13, 14). γ-AChRs also have a longer open channel lifetime, a smaller unitary conductance, and a lower Ca^{2+} permeability than ε-AChRs (15–17).

Fetal AChRs hold a special place in the history of ion channel biophysics. The first single channel recordings from cells were of γ-AChRs (18). They were also the first ion channels to be analyzed according to a thermodynamic cycle, which required quantifying constitutive activity in the absence of agonists (19). These pioneering studies of single channel currents from mouse myotubes led to the estimate that the unliganded gating equilibrium constant of γ-AChRs is $\sim 1.6 \times 10^{-6}$. γ-AChRs were also the first channels for which the rate and equilibrium constants for closed channel binding and liganded gating were measured (13, 20–22).

We have used improved methods of analysis to extend these studies of γ-AChRs with regard to both the rate constants and thermodynamics of activation. In adult AChRs, the two binding sites are functionally equivalent, but in the fetal subtype, the α–γ site has a higher affinity for ACh and provides more energy for gating than α–δ/ε. Simulations of end plate currents suggest the differences in activation properties between ε- and γ-AChR that may impact synaptic development.

Results

Definitions and Models. AChRs undergo a global, reversible allosteric transition between closed (C) and open channel (O) states. This complex reaction includes numerous changes in structure and dynamics at the binding sites (that set the affinity for agonist), side chains and domains throughout the protein (that set the equilibrium constant), and narrow regions of the pore (that set the ionic conductance). We use "gating" to refer to everything that happens in C↔O, either with or without agonists at the binding sites. Agonist binding to AChRs is also a complex reaction that requires both diffusion of the ligand and a change in protein conformation (23). We use "binding" to refer to everything that happens in the formation of a liganded complex. The binding and gating energies reported below are the sums of the energy changes for all of the microscopic steps within each of these multifaceted processes.

The model used for estimating the parameters is shown in Fig. 1*A*. The free energy difference, O vs. C, is ΔG_n, where n is the number of bound agonists (A). The horizontal arrows represent ligand binding at two sites. The free energy for binding to the lower-affinity C state is ΔG_{LA} (either α–γ/ε or α–δ) and the higher-affinity O state is ΔG_{HA}. ΔG_B is the net binding free energy from each ligand ($\Delta G_B = \Delta G_{HA} - \Delta G_{LA}$; really a ΔΔG). From detailed balance,

$$\Delta G_2 = \Delta G_0 + \Delta G_{B1} + \Delta G_{B2}. \quad [1]$$

The gating energy with two bound agonists is equal to the intrinsic gating energy plus the binding energy from two affinity changes. ΔG_B is proportional to the log of the coupling constant (the C vs. O equilibrium dissociation constant ratio), and ΔG_0 is proportional to the log of the allosteric constant (the gating equilibrium constant in the absence of agonists). ΔG_B is the free energy generated by the affinity change for the agonist at each transmitter binding site that ultimately contributes to the increased relative stability of A_2O vs. A_2C. We estimated binding and gating rate constants from single channel interval durations, equilibrium constants from the rate constant ratios, and energies by taking the log of the equilibrium constants [$\Delta G = -0.59 \ln K_{eq}$ (kcal/mol)].

ΔG_0^{WT}. Our first step was to estimate the energy difference between C and O with only water present at the two transmitter

Author contributions: T.K.N. and A.A. designed research; T.K.N. performed research; T.K.N. and A.A. analyzed data; and T.K.N. and A.A. wrote the paper.

The authors declare no conflict of interest.

This article is a PNAS Direct Submission.

[1]To whom correspondence should be addressed. E-mail: auerbach@buffalo.edu.

This article contains supporting information online at www.pnas.org/lookup/suppl/doi:10.1073/pnas.1308247110/-/DCSupplemental.

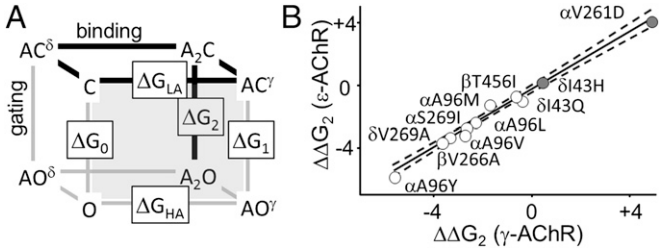

Fig. 1. Models and mutations. (*A*) Front plane is a thermodynamic cycle for one binding site. Thick lines are the physiological two-site scheme. (*B*) Side chain substitutions at homologous positions in ε- and γ-AChRs are equivalent. Plot of $\Delta\Delta G_2$ (kcal/mol) in fetal vs. adult AChRs for 11 different point mutations (open, choline; filled, ACh). Locations of the residues are shown in Fig. S1*A*. Slope of the regression = 0.93 ± 0.04 (R^2 = 0.98).

binding sites. It is difficult to estimate ΔG_0^{WT} directly, because without agonists, WT γ-AChRs rarely open. However, by using combinations of background mutations that increase constitutive activity, it is possible to estimate ΔG_0^{WT} by extrapolation (24, 25). If the only effect of each mutation is to make ΔG_0 less positive (more favorable for opening) and if each mutation acts independently, then ΔG_0^{WT} can be estimated from measurements of their effects on the energy of diliganded gating ($\Delta\Delta G_2$).

$\Delta\Delta G_2$ values have previously been measured for many different ε-AChR mutants; however, it was necessary to repeat these experiments using γ-AChRs, because the energetic consequences of the ε→γ-subunit replacement are unknown and could be global. We measured $\Delta\Delta G_2$ in γ-AChRs having 1 of 11 different background mutations (Fig. 1*B* and Fig. S1). The side chain substitutions had approximately the same effects in both receptor subtypes (Table S1).

Fig. 2*A* shows the effects of a background mutation on unliganded gating of γ-AChRs. In ε-AChRs, the mutation αA96H increases E_0 by 117,000-fold ($\Delta\Delta G_0$ = −6.4 kcal/mol) but has no effect on ΔG_B, and from the results shown in Fig. 1*B*, we assume that it has the same quantitative effect in γ-AChRs. This mutation produced clustered openings in ε-AChRs and increased constitutive activity in γ-AChRs but not enough to form clusters. One possible explanation for this difference is that ΔG_0^{WT} is more positive in γ- vs. ε-AChRs.

We measured the effect of many background mutations on unliganded γ-AChR gating calibrated alone by $\Delta\Delta G_2^{choline}$ (Fig. S1*C*). Fig. 2*B* shows a plot of the observed ΔG_0 vs. the expected $\Delta\Delta G_2$ values (−100 mV) (Fig. S2 and Table S2). If the two assumptions (independence and no effect on ΔG_B) were perfect, we expect a straight line with slope of one and a *y* intercept equal to ΔG_0^{WT}. The slope was 1.01 ± 0.03, which verifies the assumptions. The *y* intercept was $\Delta G_0^{WT\gamma}$ = + 9.9 ± 0.3 kcal/mol. For comparison, similar results for ε-AChRs are also shown and give the estimate $\Delta G_0^{WT\varepsilon}$ = + 8.3 ± 0.2 kcal/mol (25). The intrinsic free energy of gating at −100 mV is, indeed, less favorable for γ- vs. ε-AChRs. At physiological membrane potentials, the unliganded gating equilibrium constant of fetal AChRs is smaller than the unliganded gating equilibrium constant of adult AChRs (Table 1).

In ε-AChRs, hyperpolarization by −100 mV makes ΔG_0 more favorable by −1.1 kcal/mol. Therefore, in ε-AChRs, the intrinsic chemical energy for gating (at 0 mV) is +9.4 kcal/mol. Diliganded γ-AChRs show less voltage sensitivity than adult type (13), and therefore, we explored the possibility that the unliganded gating energy difference between subtypes at −100 mV was from a difference in voltage sensitivity. Fig. 2*B*, *Inset* shows that, in γ-AChRs, hyperpolarization by −100 mV increases the diliganded gating equilibrium constant by approximately e-fold, which corresponds to an energy of only ∼−0.6 kcal/mol. Hence, the intrinsic chemical energy for gating (at 0 mV) of γ-AChRs is +10.5 kcal/mol. Some but not all of the offset in the γ- vs. ε-lines in Fig. 2*B* can be attributed to different voltage sensitivities of the two subtypes.

Fig. 2*C* shows constitutive activity of WT γ-AChRs measured in the absence of agonists at −100 mV. From the distribution of open interval durations, b_0^{WT} = 2,546 ± 635 s^{-1} (mean open time ∼ 400 μs). E_0^{WT} is the ratio of the forward/backward gating rate constants, and therefore, we calculate that $f_0^{WT} = 1.32 \times 10^{-4}$ s^{-1} (each unliganded γ-AChR opens spontaneously about 11 times/d). For comparison, the gating rate constants at −100 mV in ε-AChRs are $f_0^{WT} = 67 \times 10^{-4}$ s^{-1} (∼600 times/d) and b_0^{WT} = 8,800 s^{-1} (mean open time ∼ 110 μs) (Table 2). The γ→ε-subunit substitution increases both the forward and backward gating rate constants but to different extents; therefore, the unliganded gating equilibrium constant is also increased.

ΔG_2^{ACh} and ΔG_B^{ACh}. We next measured the total energy from the affinity changes for ACh at both the α−δ and α−γ binding sites. Our approach was to measure ΔG_2^{ACh}, and then, armed with knowledge to ΔG_0^{WT}, we calculate $(\Delta G_{B1}^{ACh} + \Delta G_{B2}^{ACh})$ using Eq. **1**. At high [ACh], intracluster activity reflects mainly $A_2C \leftrightarrow A_2O$ gating. To facilitate gating rate constant measurements, we depolarized the membrane to +70 mV (to reduce channel block by the agonist) and added background mutations that increased ΔG_0 (to decrease f_2^{ACh}) but did not affect ΔG_B^{ACh} (Table S1) (26). Fig. 3*A* shows example single channel currents at several different [ACh]. The slowest shut component within clusters reached an asymptote at ∼1 mM [ACh] (Fig. 3*B*). We estimated the gating rate constants in this background construct by fitting

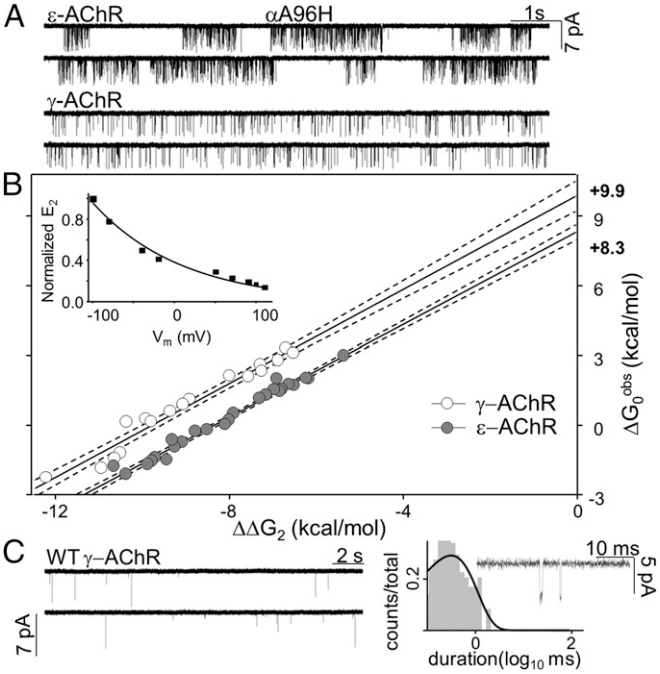

Fig. 2. The intrinsic gating energy of γ-AChRs. (*A*) Low-resolution view of unliganded single channel currents in AChRs having αA96H mutations (both α-subunits). ε-AChR currents are clustered, whereas those currents from γ-AChRs are not. (*B*) Correlation plot of the expected $\Delta\Delta G_2$ vs. the observed ΔG_0. Open, γ-AChRs; filled, ε-AChRs. Slopes and *y* intercepts: γ-AChRs, 1.01 ± 0.034 and 9.9 ± 0.3 kcal/mol; ε-AChRs, 0.996 ± 0.02 and 8.32 ± 0.16 kcal/mol. (*Inset*) Diliganded gating equilibrium constant (E_2) vs. membrane voltage (V_m) for γ-AChRs (background: βT456I + δI43H). E_2^{ACh} decreases e-fold with 109 ± 7.2 mV depolarization. (*C*, *Left*) Low-resolution single channel currents from unliganded WT γ-AChRs. (*C*, *Right*) Corresponding open-time histogram. (*Inset*) Higher-resolution view of the trace in *C*, *Left*.

Table 1. Equilibrium constants and free energies

Site	Equilibrium constants			Free energies (kcal/mol)		
		Fetal	Adult		Fetal	Adult
—	E_0	5.2×10^{-8}	7.6×10^{-7}	ΔG_0	+9.9	+8.3
α–ε/δ	E_1	6.4×10^{-4}	4.3×10^{-3}	ΔG_1	+4.3	+3.2
α–γ	E_1	8.0×10^{-3}	—	ΔG_1	+2.9	—
Both	E_2	59	25	ΔG_2	−2.4	−1.9
α–ε/δ	K_d	179 μM	166 μM	ΔG_{LA}	−5.1	−5.1
α–ε/δ	J_d	24 nM	25 nM	ΔG_{HA}	−10.3	−10.3
α–ε/δ	K_d/J_d	7,460	6,000	ΔG_B	−5.5	−5.1
α–γ	K_d	8.0 μM	—	ΔG_{LA}	−6.9	—
α–γ	J_d	0.15 nM	—	ΔG_{HA}	−13.4	—
α–γ	K_d/J_d	50,000	—	ΔG_B	−7.1	—

E_n, gating equilibrium constant with n bound ACh; K_d and J_d, ACh equilibrium dissociation constants of C and O.

the interval durations obtained only at 10 mM ACh, with the result $f_2^{ACh,\,bkg} = 3{,}565 \pm 195\ s^{-1}$ and $b_2^{ACh,\,bkg} = 807 \pm 59\ s^{-1}$ (Table S3).

To obtain the values pertaining to WT γ-AChRs, we corrected for background perturbations simply by multiplying the observed rate constants by the fold changes incurred for each perturbation alone (Table S1). We estimate that, in WT γ-AChRs (−100 mV), $f_2^{ACh} = 24{,}020 \pm 776\ s^{-1}$ and $b_2^{ACh} = 410 \pm 17\ s^{-1}$ or $(f_2/b_2)^{ACh} = 58.7 \pm 3.1$ and $\Delta G_2^{ACh} = -2.4 \pm 0.04$ kcal/mol. The corresponding values in ε-AChRs are shown in Tables 1 and 2. γ-AChRs have a slightly higher diliganded gating equilibrium constant and hence, generate a slightly higher maximum open probability (P_O^{max}) from the neurotransmitter.

Because we had estimates for both ΔG_2^{ACh} and ΔG_0 in WT γ-AChRs, we could calculate the total energy from both binding sites generated by the two lower-affinity (LA) →higher-affinity (HA) changes for the neurotransmitter (Eq. **1**). The result was $(\Delta G_{B1} + \Delta G_{B2}) = -12.4$ kcal/mol. For comparison, in ε-AChRs, this sum is −10.2 kcal/mol (10). Although ΔG_0^{WT} (−100 mV) is less favorable for opening in γ-AChRs, the combined energy from the affinity changes for ACh at the two binding sites is more favorable and makes the diliganded gating equilibrium constant slightly larger.

In ε-AChRs, the α–ε and α–δ transmitter binding sites each provide approximately the same energy from the affinity change, $\Delta G_B^{ACh} = -5.1$ kcal/mol (27). To make this separation in γ-AChRs, we studied receptors that gate normally but are capable of using ligand energy from only one of two binding sites.

Table 2. Rate constants ($s^{-1}/M^{-1}s^{-1}$)

Site		Fetal	Adult
	f_0	1.3×10^{-4} (8×10^{-5})	6.7×10^{-3}
	b_0	2,550 (635)	8,800
α–δ	f_1	3.4 (0.04)	3.4
α–δ	b_1	5,160 (38)	5,160
α–γ/ε	f_1	12 (0.2)	3.4
α–γ/ε	b_1	1,460 (30)	5,160
Both	f_2	24,020 (780)	65,850
Both	b_2	410 (17)	2,595
α–δ	k_{on}	—	1.1×10^8
α–δ	k_{off}	—	20,000
α–δ	j_{on}	—	1×10^9
α–δ	j_{off}	—	24
α–γ/ε	j_{on}	5.6×10^{10} (3×10^9)	1×10^9
α–γ/ε	j_{off}	8.5 (0.6)	24

Values in parentheses are ± SEM. b_n, backward O→C; f_n, forward C→O; k and j, ACh binding rates to C and O.

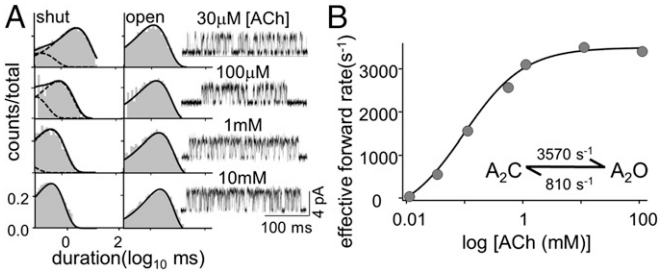

Fig. 3. Estimating the diliganded gating energy ΔG_2^{ACh}. (*A*) Interval duration histograms and example currents at different [ACh] (background mutations, βT456I + δI43H; +70 mV). (*B*) The effective forward rate asymptotes at ~1 mM ACh. The corresponding P_O vs. [ACh] plot is shown in Fig. 4*D*. (*Inset*) Gating rate constants estimated at 10 mM ACh ($n = 3$ patches). Depolarization by +170 mV, βT456I and δI43H decrease f_0 (1.4-, 0.9-, and 5.1-fold, respectively; combined effect, 6.75-fold) and increase b_0 (0.3-, 3.3-, and 0.5-fold, respectively; combined effect, 0.51-fold). The observed rate constants were multiplied by the combined effect to arrive at the rate constants for WT γ-AChRs at −100 mV: $f_2^{ACh} = 24{,}020\ s^{-1}$ and $b_2^{ACh} = 410\ s^{-1}$ ($E_2^{ACh,WT} = 58.7$ and $\Delta G_2^{ACh,WT} = -2.4$ kcal/mol).

In the first approach, we used the mutation αW149M (of a conserved binding site residue) that, in ε-AChRs, effectively eliminates the ability of ACh to bind and provide energy to gating (10). With both binding sites mutated in this way, activity of γ-AChRs in 500 μM ACh was attenuated compared with the WT, indicating that binding energy had been reduced substantially (Fig. 4*A*, *Left*). We needed to measure the effects of this mutation on ΔG_0, and therefore, we added additional background mutations to increase constitutive activity to a level sufficient to generate unliganded clusters of openings (*SI Methods*). As was the case with ε-AChRs, the two αW149M mutations together only changed ΔG_0 modestly by −0.4 kcal (Fig. 4*A*, *Right* and Table S2).

To make hybrid γ-AChRs (with one functional binding site), we cotransfected WT and W149M α-subunits along with WT β-, δ-, and γ-subunits. We expected four different AChR populations to be expressed: MM (double KO), MW, WM (single KO), and WW (WT), where the letters represent the αW149 side chain at α–γ and α–δ. Indeed, in 500 μM ACh, four types of clusters were apparent in the single channel currents (Fig. 4*B*). The highest and lowest P_O populations represent WW (WT) and MM γ-AChRs, whereas the two intermediate ones are MW and WM (Fig. 4*C*). Because the αW149M mutation hardly changes ΔG_0 (Table S2), the P_O difference between these populations is from different ΔG_B^{ACh} values at the two binding sites.

Each cluster population was analyzed separately to obtain f_1^{ACh}, b_1^{ACh}, and ΔG_1^{ACh}. The calculated ΔG_B^{ACh} value for each site ($= \Delta G_1^{ACh} - \Delta G_0$) was -7.1 ± 0.32 kcal/mol for the higher P_O hybrid population and -5.5 ± 0.3 kcal/mol from the lower P_O hybrid population (Table S4). This result confirms that, with ACh, the two binding interfaces in γ-AChRs are asymmetric. One of the ΔG_B^{ACh} values is approximately the same as the α–δ site in ε-AChRs (−5.1 kcal/mol), and therefore, we provisionally associate the more negative value with the α–γ binding site.

To test this association, we used a different KO mutation (Fig. 4*D*). In ε-AChRs, the mutation δP123R on the non-α side of the binding pocket effectively eliminates binding and activation at α–δ (28). We first measured the effect of this mutation on ΔG_0 in γ-AChRs and found it to be the same as in ε-AChRs (Table S2). We then measured ACh-activated single channel current clusters from γ-AChRs having this mutation, and hence, only the α–γ binding site is operational. The Hill coefficient of the single channel dose–response curve was $\alpha_H = 0.74$, indicating that only a single binding site was functional. After correcting for all backgrounds, we estimate that $\Delta G_{B\gamma}^{ACh} = -7.2$ kcal/mol, which agrees with the estimate from the higher P_O hybrid.

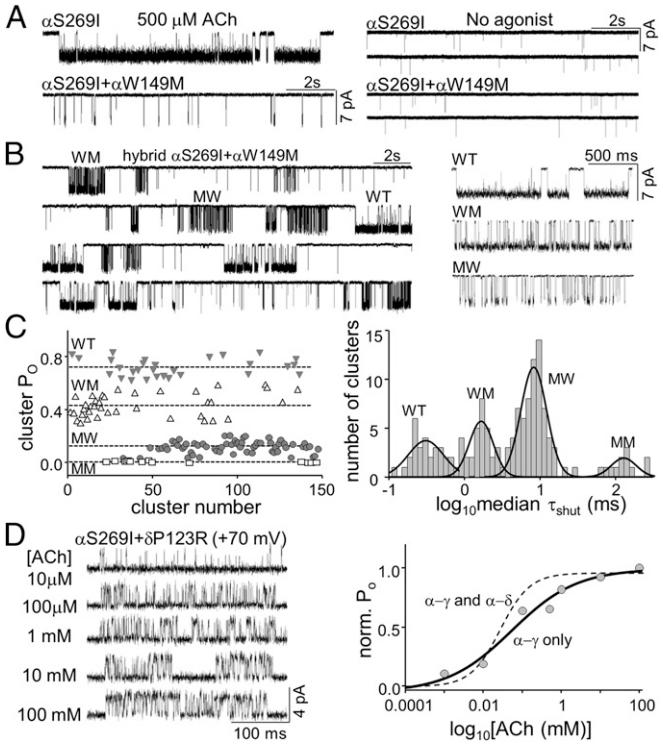

Fig. 4. Activation of γ-AChRs having only one functional binding site. (*A*, *Left*) In presence of ACh, αW149M KO mutation (at both binding sites) attenuates diliganded gating of γ-AChRs (background mutation, αS269I; −100 mV), because the binding sites are unable to use the energy from agonist binding. (*A*, *Right*) αW149M mutation does not affect unliganded gating. (*B*, *Left*) Continuous single channel current trace showing activity from WT, two different hybrids (one αW149 mutated; MW or WM), and double-αW149M mutant (MM; 500 μM ACh, −100 mV). (*B*, *Right*) Higher-resolution view of the marked clusters in *B*, *Left*. Note the difference in P_O between WM and MW. (*C*, *Left*) Distribution of clusters based on P_O. The populations correspond to MM, MW, WM, and WT γ-AChRs (dotted line, mean population P_O). (*C*, *Right*) Distribution of clusters based on median shut lifetime (τ_{close}). (*D*, *Left*) Single channel current from γ-AChRs containing δP123R KO mutation at α–δ binding site (+70 mV). αS269I increases single channel activity by reducing ΔG_0. (*D*, *Right*) Plot of normalized P_O vs. [ACh] fitted to Hill equation. Solid line, $\alpha_H = 0.74 \pm 0.2$ ($R^2 = 0.94$; only α–γ site functional); dotted line, both α–γ and α–δ sites functional (Fig. 3).

The results show that the α–γ binding site provides an extra ∼−2.1 kcal/mol from the affinity change for ACh compared with the α–δ binding site. Without this additional energy, the diliganded gating equilibrium constant of γ-AChRs would be ∼30 times smaller.

Transmitter Binding. In ε-AChRs, the two transmitter binding sites have approximately the same LA equilibrium dissociation constant for ACh ($K_d^{ACh} \sim 166$ μM), which is the ratio of the dissociation/association rate constants $k_{off}^{ACh} = 19,969$ s^{-1} and $k_{on}^{ACh} = 121$ $\mu M^{-1}s^{-1}$ (10). We measured K_d^{ACh} and the binding rate constants for the α–γ site using the single site KO method (Fig. 5*A*).

The KO mutations were δP123R plus δW57A, another residue on the non-α side of the binding pocket that has been characterized previously in ε-AChRs (29). In γ-AChRs, the δP123R + δW57A combination nearly abolished activation by 500 μM ACh. To estimate K_d^{ACh} at α–γ, we fitted single channel currents in AChRs having these δ-subunit mutations across a range of [ACh] by using a sequential A + C↔AC↔AO scheme (Fig. 1*A*, front plane). The result was that, at the α–γ site, $K_d^{ACh} = 8.0$ μM, $k_{off}^{ACh} = 1,794$ s^{-1}, and $k_{on}^{ACh} = 225$ $\mu M^{-1}s^{-1}$. From the fit, we also obtained the estimate $\Delta G_1^{ACh} = +2.9$ kcal/mol. We now calculate that $\Delta G_{B2}^{ACh} = -7.0$ kcal/mol, which is in good agreement with the value obtained by the hybrid and KO methods that used different background mutations.

In ε-AChRs, the two transmitter binding sites also have approximately the same HA equilibrium dissociation constant for ACh ($J_d^{ACh} \sim 25$ nM). We estimated J_d^{ACh} as well as the HA on and off rate constants (j_{on} and j_{off}) for γ-AChRs from kinetic modeling of single channel currents (30). We used the α–δ KO mutations (δP123R) plus two additional mutations in the pore (βL262S and γL260Q) that reduced ΔG_0 and caused openings from constitutively active γ-AChR to occur in clusters (Fig. 5*B*). To complete the characterization of this background, we also had to consider desensitization. AChRs enter short-lived desensitized states both with and without agonists at the binding sites (31). We measured the entry and exit rates for such sojourns, and therefore, these events would not be mistaken for events from the binding–gating cycle. The entry and exit rate constants pertaining to short-lived desensitization were 19 and 3,324 s^{-1} (Fig. S3). In WT ε-AChRs, these rate constants are 23 and 277 s^{-1}. We suspect that the ∼10-fold difference in recovery rate constant arises from the background pore mutations, but it is possible that ε→γ subunit substitution also had an effect.

To measure HA binding to O, we exposed AChRs having the background mutations to very low [ACh] (≤1 nM) (Fig. 5*B*). Under this experimental condition, activation mainly occurred by the A + C↔A + O↔AO pathway rather than by A + C↔A-C↔AO (Fig. 1*A*, front plane). We fitted the intracluster intervals durations using the first of these schemes, with the results of $j_{off}^{ACh} = 8.5$ s^{-1}, $j_{on}^{ACh} = 56$ $nM^{-1}s^{-1}$, and $J_d^{ACh} = 0.15$ nM. Brief sojourns in the short-lived desensitized state were apparent at low [ACh], but intervals arising from sojourns in AC were not apparent, because their lifetime is too brief (∼500 ns) to be detected by the patch-clamp method.

Discussion

Structure and Energy. At −100 mV and with ACh present at both transmitter binding sites, the A_2O vs. A_2C energy difference is similar for both AChR subtypes (∼−2 kcal/mol). However, this end result is achieved in different ways. Compared with α–δ and α–ε, the α–γ binding site provides extra binding energy ($\Delta\Delta G_B = -2.2$ kcal/mol) that offsets the larger unliganded chemical gating energy gap ($\Delta\Delta G_0 = +0.9$ kcal/mol) and weaker voltage dependence ($\Delta\Delta G_{-0.1V} = +0.5$ kcal/mol) of γ-AChRs.

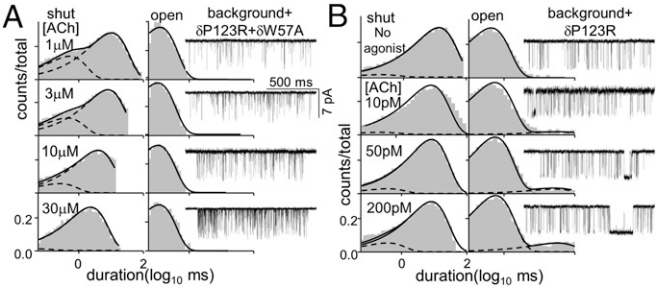

Fig. 5. Estimating the C and O affinities for ACh at the α–γ binding site. (*A*) Interval duration histograms and example clusters at different [ACh]. The δ-subunit mutations knocked out activation by α–δ (αA96V + βT456I added to boost single channel activity by decreasing ΔG_0). Solid curves are the global fit (dotted lines, exponential components) to scheme A + C↔AC↔AO (Fig. 1*A*). (*B*) Interval duration histograms and example clusters at less than nanomolar [ACh]. The δ-subunit mutation knocked out activation by α–δ (background mutations: βL262S + γL260Q). Solid curves are the global fit to scheme A + C↔A + O↔AO (Fig. 1*A*). The dashed lines in the shut histograms are fast desensitization components, and in the open histograms, they are rare monoliganded gating activities.

Without the energy boost from α−γ, the maximum P_O^{ACh} in fetal-type AChRs would be only 0.38 rather than 0.98.

Aside from the extra binding energy from α−γ, adult and fetal AChRs are remarkably similar considering that the ε- and γ-subunits have only 52% sequence identity (~260 side chain substitutions). Because many mutations throughout the protein can change ΔG_0 substantially, this similarity suggests that the unliganded ground state energies of the two subtypes have been selected to be appropriate for their physiological roles. The effects of many mutations on ΔG_0 are the same in γ- and ε-AChRs (Fig. 1*B*), which indicates that the overall gating mechanism is not altered by the subunit swap. Also, the fact that ΔG_B^{ACh} is the same at α−δ, regardless of whether the other site is α−ε or α−γ, attests to the essential independence of the two transmitter binding sites (28). These observations are consistent with the view that, in AChRs, the side chains mainly set the unliganded O vs. C ground state energy difference by local resettling and are not the principle agents of site↔gate communication (32).

The sources of the extra binding energy from α−γ are not known. In ε-AChRs, three binding site groups (an "aromatic triad") in the α-subunit (αW149, αY190, and αY198) each provide ~−2 kcal/mol to the increased stabilization of ACh in the HA vs. LA complex (33). Two other aromatic residues, αY93 and ε/δW57/55 (on the non-α surface of the binding pocket), are nearby but contribute little or nothing to ΔG_B^{ACh}. It is possible that the extra α−γ energy comes from increased stabilization by these side chains or others on the γ-side of the pocket, increased binding energy from members of the aromatic triad, or perhaps, decreased unfavorable coupling energy between triad members. It will be interesting to learn the sources of ACh binding energy at the α−γ site as well as this accounting for other agonists, including the ACh breakdown product choline.

The ε→γ subunit replacement has a partial catalytic effect on gating. Both f_0 and b_0 are increased but unequally (by 50- and 4-fold, respectively). The greater effect on the forward rate constant suggests that some of the residue substitutions in the γ-subunit that alter ΔG_0 are in regions of the protein that mainly influence f_0, perhaps of the same amino acids at the α−γ binding site that are responsible for the increase in ΔG_B^{ACh}. For diliganded gating with ACh, the ε→γ subunit replacement is also catalytic, but the rate constant ratios are smaller and more similar (~2.5- and ~5-fold). The affinity change for the agonist (ΔG_B) contributes to the diliganded gating equilibrium constant by rearrangements at the binding site that mainly effect f_2 (high-ϕ) (32).

The greater voltage sensitivity of ε- vs. γ-AChRs is small and may reflect a change in the net dipole of the entire 20-helix transmembrane domain rather than a difference in discrete charged amino acids. A small change in the tilt angles of the ε- vs. γ-AChR transmembrane helices could be sufficient to generate the ~−0.5 kcal/mol energy difference.

With regard to LA binding, K_d^{ACh} at α−γ was ~20 times lower than at α−δ or α−ε, mainly because of an ~10 times smaller k_{off}^{ACh}. The γ-side chains responsible for this affinity difference are not known. The higher resting affinity of α−γ vs. α−ε is opposite of what was observed in competitive assays of carbamylcholine binding to desensitized *Torpedo* AChRs (34). In the same study, α−γ had a higher affinity for the competitive antagonist d-tubocurarine compared with α−δ.

In energy units, the ε/δ→γ K_d^{ACh} ratio is equivalent to $\Delta\Delta G_{LA} = -1.8$ kcal/mol, which is about the same as the $\Delta\Delta G_B^{ACh}$ difference. That is, LA binding is more favorable at α−γ vs. α−ε/δ, and HA binding is even more favorable ($\Delta\Delta G_{HA} = -3.0$ kcal/mol). This result is consistent with previous results showing a correlation between LA and HA binding affinities in ε-AChRs, with a $\Delta\Delta G_{LA}/\Delta\Delta G_{HA}$ ratio of ~0.5 (23). This correlation suggests that LA binding and the LA→HA switch are stages of a single integrated mechanism called catch and hold. Apparently, this set of molecular rearrangements occurs at α−γ as well as α−δ and α−ε.

The kinetics and energetics of synaptic AChRs have been optimized by natural selection. Jackson (35) predicted that the optimal unliganded gating equilibrium constant should be $\sim 10^{-6}$ and that the binding sites should be unequal in their affinities to maximize the available binding energy from ACh. Jackson (35) also predicted an equilibrium dissociation constant from the open conformation of ~0.14 nM. The results described above corroborate the predictions by Jackson (35). γ-AChRs optimally use the energy from neurotransmitter binding during synaptogenesis.

Synaptic Currents. Knocking out the expression of γ is lethal. This outcome may result from ε- vs. γ-AChR properties other than what we have quantified (binding and gating; for example, from a mismatch between muscle fiber impendence and AChR kinetics). Here, we only consider how the rate and equilibrium constants for the two subtypes might affect synapses. It is important to note that both binding and gating constants change substantially with temperature (36), and therefore, without additional experiments, we cannot extrapolate our 23 °C results to what happens in mice at 39 °C.

The properties of ε- vs. γ-AChRs (Table 1) should result in ~18 times larger unliganded (leak) current and ~40-fold higher resting Ca^{2+} influx (17). If ε-AChRs are expressed at extrajunctional sites, the greater Ca^{2+} influx could affect synapse development. Although unliganded openings at −100 mV are less frequent in γ- vs. ε-AChRs, they are longer-lived. In effect, in the absence of ligands, the fetal subtype produces a higher signal-to-noise ratio, despite the lower single channel conductance. It is possible, but not likely, that this difference in unliganded gating is of physiological significance.

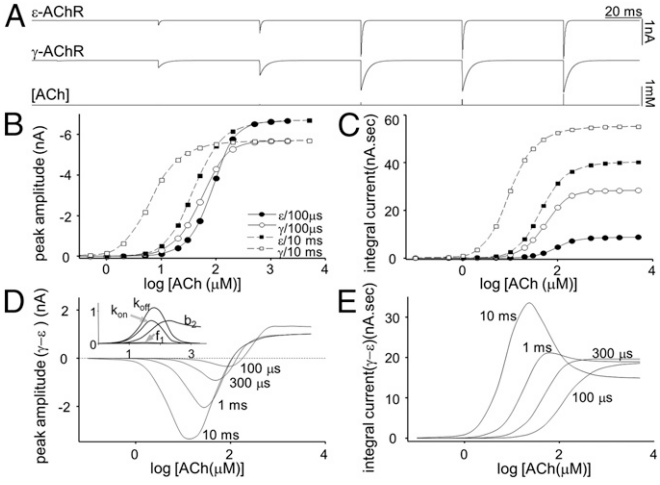

Fig. 6. Simulations of mEPCs using ε- and γ-AChR rate constants. (*A*) Simulated mEPCs using the model shown in Fig. 1*A* and rate constants shown in Table 2 (pulse duration = 0.1 ms). At high [ACh], the ε-AChR response is larger because of its larger conductance. At all [ACh], the γ-AChR response is slower because of its slower b_2^{ACh}. (*B*) Plot of peak amplitude vs. [ACh] at two pulse durations: 100 μs (solid curve) and 10 ms (dotted curve). γ-AChR responses (open symbols) are left-shifted from ε-AChR (filled symbols). (*C*) Plot of the integrated mEPC vs. [ACh]. The shifts in the γ- vs. ε- responses are exaggerated compared with peak responses (*B*). (*D*) Plot of the difference in peak amplitude (γ − ε) vs. [ACh] at different pulse durations (negative currents are larger). (*Inset*) Plot of the peak difference when f_1, b_2, k_{on}, and k_{off} are changed from γ- to ε-AChR values (Table 2). The major effects are from k_{off} and b_2. (*E*) Plot of the difference in integral current (γ − ε) vs. [ACh] at different stimulus durations. In both *D* and *E*, the difference is greatest between 60 and 120 μM.

More probable is that it is the difference in the liganded response between AChR subtypes that pertains to survival. It is well-known that, at high synaptic peak [ACh], adult responses are larger and briefer than fetal ones. We were interested to learn how the ~10-fold slower k_{off}^{ACh}, the ~4-fold faster f_1^{ACh}, and the approximately ~8-fold slower b_2^{ACh} in γ- vs. ε-AChRs together impact synaptic currents. Fig. 6 shows the results of simulations of miniature end plate currents (mEPCs) for each subtype using the model in shown in Fig. 1*A* and the rate constants in Table 2. The simulations were for 1,000 AChRs at −100 mV, and they incorporated the difference in the single channel current amplitude (−5.5 vs. −7.0 pA, γ vs. ε). In the simulations, both the concentration and duration of the rectangular ACh pulses were varied.

Fig. 6*A* shows simulated mEPCs using pulse duration of 0.1 ms at different [ACh]. At lower [ACh], the peak response from γ-AChRs is larger than from ε-AChRs because of the higher affinity for ACh at α−γ vs. α−ε. At high [ACh], this effect disappears, and the peak response from ε-AChR is larger because of the larger single channel conductance. At all concentrations, deactivation of γ-AChR is slower because of the slower channel closing rate constant.

Fig. 6 *B* and *C* shows the peak and integrated responses at different [ACh], with 100-μs and 10-ms (steady state) pulses. The results are summarized in Fig. 6 *D* and *E*, which shows the differences as γ- − ε-AChRs. With regard to the peak response, the peak responses from γ-AChRs are larger at [ACh] between 60 and 120 μM, with the difference increasing and the [ACh] at the maximum difference decreasing as the pulse gets longer. The same pattern holds for the integrated response. The γ-AChRs generate significantly larger synaptic currents under conditions where [ACh] is in the range from 60 to 120 μM and the synaptic pulse durations are >0.3 ms. At submicromolar [ACh], only γ-AChRs generated mEPCs, largely because of the slow k_{off} at the α−γ binding site (Fig. 6*D*, *Inset*).

The peak [ACh] at the adult neuromuscular synapse has been estimated to be ~1 mM. However, during the course of synaptic development, the amount of ACh released per vesicle could be smaller, the synaptic gap could be wider, or the amount of cholinesterase could be greater. Any of these changes would lower the synaptic [ACh]. If the synaptic [ACh] was 60–160 μM, only γ-AChRs would generate significant inward currents in muscle cells. We speculate that it may be the ability of γ-AChRs to be activated by lower ACh that is, in turn, determined by the lower K_d^{ACh} and more favorable ΔG_B^{ACh} at the α−γ site that allows proper synapse formation.

Methods

Mouse AChR subunit cDNAs were mutated by the QuikChange Site-Directed Mutagenesis Kit (Agilent Technologies). HEK cells were transfected by calcium phosphate precipitation and used for cell-attached patch-clamp recordings. Kinetic rate and equilibrium constants were estimated from single-channel interval durations (*SI Methods*).

ACKNOWLEDGMENTS. We thank M. Merritt, M. Shero, M. Teeling, C. Nicolai, and Dr. S. Gupta. This work was funded by National Institutes of Health Grants R37 NS-23513 and NS-064969.

1. Missias AC, Chu GC, Klocke BJ, Sanes JR, Merlie JP (1996) Maturation of the acetylcholine receptor in skeletal muscle: Regulation of the AChR gamma-to-epsilon switch. *Dev Biol* 179(1):223–238.
2. Borodinsky LN, Spitzer NC (2007) Activity-dependent neurotransmitter-receptor matching at the neuromuscular junction. *Proc Natl Acad Sci USA* 104(1):335–340.
3. Liu Y, Sugiura Y, Padgett D, Lin W (2010) Postsynaptic development of the neuromuscular junction in mice lacking the gamma-subunit of muscle nicotinic acetylcholine receptor. *J Mol Neurosci* 40(1–2):21–26.
4. Koenen M, Peter C, Villarroel A, Witzemann V, Sakmann B (2005) Acetylcholine receptor channel subtype directs the innervation pattern of skeletal muscle. *EMBO Rep* 6(6):570–576.
5. Jin TE, Wernig A, Witzemann V (2008) Changes in acetylcholine receptor function induce shifts in muscle fiber type composition. *FEBS J* 275(9):2042–2054.
6. Takahashi M, et al. (2002) Spontaneous muscle action potentials fail to develop without fetal-type acetylcholine receptors. *EMBO Rep* 3(7):674–681.
7. Vogt J, et al. (2012) CHRNG genotype-phenotype correlations in the multiple pterygium syndromes. *J Med Genet* 49(1):21–26.
8. Morgan NV, et al. (2006) Mutations in the embryonal subunit of the acetylcholine receptor (CHRNG) cause lethal and Escobar variants of multiple pterygium syndrome. *Am J Hum Genet* 79(2):390–395.
9. Hoffmann K, et al. (2006) Escobar syndrome is a prenatal myasthenia caused by disruption of the acetylcholine receptor fetal gamma subunit. *Am J Hum Genet* 79(2):303–312.
10. Jha A, Auerbach A (2010) Acetylcholine receptor channels activated by a single agonist molecule. *Biophys J* 98(9):1840–1846.
11. Auerbach A, Lingle CJ (1987) Activation of the primary kinetic modes of large- and small-conductance cholinergic ion channels in Xenopus myocytes. *J Physiol* 393:437–466.
12. Sine SM, Steinbach JH (1987) Activation of acetylcholine receptors on clonal mammalian BC3H-1 cells by high concentrations of agonist. *J Physiol* 385:325–359.
13. Sine SM, Claudio T, Sigworth FJ (1990) Activation of Torpedo acetylcholine receptors expressed in mouse fibroblasts. Single channel current kinetics reveal distinct agonist binding affinities. *J Gen Physiol* 96(2):395–437.
14. Andreeva IE, Nirthanan S, Cohen JB, Pedersen SE (2006) Site specificity of agonist-induced opening and desensitization of the Torpedo californica nicotinic acetylcholine receptor. *Biochemistry* 45(1):195–204.
15. Mishina M, et al. (1986) Molecular distinction between fetal and adult forms of muscle acetylcholine receptor. *Nature* 321(6068):406–411.
16. Herlitze S, Villarroel A, Witzemann V, Koenen M, Sakmann B (1996) Structural determinants of channel conductance in fetal and adult rat muscle acetylcholine receptors. *J Physiol* 492(Pt 3):775–787.
17. Villarroel A, Sakmann B (1996) Calcium permeability increase of endplate channels in rat muscle during postnatal development. *J Physiol* 496(Pt 2):331–338.
18. Neher E, Sakmann B (1976) Single-channel currents recorded from membrane of denervated frog muscle fibres. *Nature* 260(5554):799–802.
19. Jackson MB (1984) Spontaneous openings of the acetylcholine receptor channel. *Proc Natl Acad Sci USA* 81(12):3901–3904.
20. Colquhoun D, Sakmann B (1985) Fast events in single-channel currents activated by acetylcholine and its analogues at the frog muscle end-plate. *J Physiol* 369:501–557.
21. Sine SM, Steinbach JH (1986) Activation of acetylcholine receptors on clonal mammalian BC3H-1 cells by low concentrations of agonist. *J Physiol* 373:129–162.
22. Jackson MB (1988) Dependence of acetylcholine receptor channel kinetics on agonist concentration in cultured mouse muscle fibres. *J Physiol* 397:555–583.
23. Jadey S, Auerbach A (2012) An integrated catch-and-hold mechanism activates nicotinic acetylcholine receptors. *J Gen Physiol* 140(1):17–28.
24. Purohit P, Auerbach A (2009) Unliganded gating of acetylcholine receptor channels. *Proc Natl Acad Sci USA* 106(1):115–120.
25. Nayak TK, Purohit PG, Auerbach A (2012) The intrinsic energy of the gating isomerization of a neuromuscular acetylcholine receptor channel. *J Gen Physiol* 139(5):349–358.
26. Jadey SV, Purohit P, Bruhova I, Gregg TM, Auerbach A (2011) Design and control of acetylcholine receptor conformational change. *Proc Natl Acad Sci USA* 108(11):4328–4333.
27. Auerbach A (2010) The gating isomerization of neuromuscular acetylcholine receptors. *J Physiol* 588(Pt 4):573–586.
28. Gupta S, Purohit P, Auerbach A (2013) Function of interfacial prolines at the transmitter-binding sites of the neuromuscular acetylcholine receptor. *J Biol Chem* 288(18):12667–12679.
29. Bafna PA, Purohit PG, Auerbach A (2008) Gating at the mouth of the acetylcholine receptor channel: Energetic consequences of mutations in the alphaM2-cap. *PLoS One* 3(6):e2515.
30. Purohit P, Auerbach A (2013) Loop C and the mechanism of acetylcholine receptor-channel gating. *J Gen Physiol* 141(4):467–478.
31. Elenes S, Auerbach A (2002) Desensitization of diliganded mouse muscle nicotinic acetylcholine receptor channels. *J Physiol* 541(Pt 2):367–383.
32. Auerbach A (2013) The energy and work of a ligand-gated ion channel. *J Mol Biol* 425(9):1461–1475.
33. Purohit P, Bruhova I, Auerbach A (2012) Sources of energy for gating by neurotransmitters in acetylcholine receptor channels. *Proc Natl Acad Sci USA* 109(24):9384–9389.
34. Blount P, Merlie JP (1989) Molecular basis of the two nonequivalent ligand binding sites of the muscle nicotinic acetylcholine receptor. *Neuron* 3(3):349–357.
35. Jackson MB (1989) Perfection of a synaptic receptor: Kinetics and energetics of the acetylcholine receptor. *Proc Natl Acad Sci USA* 86(7):2199–2203.
36. Gupta S, Auerbach A (2011) Temperature dependence of acetylcholine receptor channels activated by different agonists. *Biophys J* 100(4):895–903.